A Fast Spectral Domain Solver for the Characterization of Larger Microwave Structures in Multilayered Environments

T. Vaupel

Research Institute for High Frequency Physics and Radar Techniques, FGAN E.V.
Neuenahrer Str. 20, 53343 Wachtberg, Germany
vaupel@fgan.de

Abstract – A new kind of fast spectral domain method is presented for the solution of integral equations related to planar structures embedded in multilayered media. It is based on the well-known spectral domain Green's function for multilayered media to construct a diagonalized translation operator on the Cartesian wavenumber plane to efficiently evaluate the matrix-vector multiplications during the iterative solution process. This allows fast integral equation solutions for arbitrary layer arrangements similar as with fast multipole methods (FMM) for structures in free space. The convergence properties of the involved spectral domain integrals related to the group interactions are drastically improved by different integration path deformation strategies combined with enhanced Legendre-Filon and Laguerre quadrature techniques. Together with the use of diakoptic preconditioners, only a small number of iterations are required with the pertinent Krylov subspace solvers, typically leading to a significantly higher computational performance than comparable commercial integral equation solvers.

Keywords: Planar-3D-structures, multilayered media, fast integral equation solver, adaptive integration path deformation, extended quadrature techniques, and diakoptic preconditioner.

I. INTRODUCTION

A large class of structures like microstrip or combined slot/microstrip configurations can be modeled as so-called Planar-3D structures embedded within multilayered medias. Using the method of moments (MoM) in combination with the Green's function of the multilayered environment reduces the discretization effort to the strip and/or slot areas of the structure. However, due to the growing complexity of microwave circuits and antennas, the number of unknowns can easily become prohibitive, if standard MoM implementations are applied. To overcome the large computational effort of the standard MoM, different fast integral equation solvers for microstrip structures have been proposed. First implementations were based on a combination of the conjugate gradient method with the fast Fourier transform (CG-FFT) for structures in free space [1,2] and its extension to microstrip structures [3]. A further extension using the discrete complex-image technique for the characterization of the layered medium was presented in [4]. Other approaches make use of the adaptive integral method (AIM) for accelerating the matrix-vector products combined as well with the complex-image technique [5]. Methods based on the fast multipole method (FMM) and complex-image techniques are given in [6,7]. However, the numerical efficiency of the complex-image technique may strongly depend on the number of required complex images. Another approach employing a fast multipole method (FMM) can be found in [8] but is restricted to a thin grounded dielectric slab. These drawbacks are partly overcome by the fast inhomogeneous plane wave algorithm, presented in [9], which is well suited for scatterers located above an arbitrary multilayered medium or for buried objects.

In contrast to these methods, an approach completely based on the spectral domain Green's function of the multilayered medium is presented in this paper. The corresponding Green's function can be easily computed for arbitrary layer/metallization arrangements with the same numerical performance and accuracy, even for problematic configurations like e.g. thin glue layers embedded in much thicker sub/superstrate environments. The method is based on the construction of a diagonalized translation operator on the cartesian wavenumber plane to compute the far interactions between non-overlapping groups of basis functions. The interactions of near-neighbour groups are computed using the matrix entries of the conventional MoM analogously to other fast integral equation formulations. The far interactions are formulated as spectral domain integrals but have bad convergence properties if only real cartesian wavenumbers are used. Thus, an extension on complex integration paths is used on one hand to circumvent singularities of the integrand [11] and on the other hand to get an exponential decay of the integrands. To achieve this decay , the proposals given in [12] are modified in such a way that the employed integration paths do not cross any singularities of the integrands. However, for large group separations the numerical efficiency is still affected by an oscillatory behavior of the integrands. These oscillations are compensated with some modifications of a Legendre-Filon quadrature given in [11] as well. Furthermore, the exponential decay

rate on the modified integration paths depends on the lateral distance of the participated groups which makes it difficult to account for the fast decay rate concerning group interactions with large lateral distances. Therefore an extended Laguerre quadrature technique is introduced which provides practically the same decay rate for all group far interactions. The overall performance of this approach is decisively improved by employing Krylov subspace solvers with extended diakoptic preconditioners [13] for the treatment of the linear systems of equations leading to a very fast convergence of the iterative solution process for a large class of structures. Since our method is still a two-level approach, the numerical complexity for the matrix-vector product evaluation reaches $\approx O(N^{1.5})$ with an optimized group size [14] whereas we get roughly $\approx O(N)$ for the storage complexity.

II. FORMULATION

A. General Outline of The Fast Algorithm

In a first step, the structure to be analyzed is decomposed into groups, which comprise typical components like couplers, patches, spiral inductors etc. (see Fig. 1). In this context, also a subsequent partitioning into small squares as in [8] may be applied, but with the risk of dissecting resonant components of the structure such as antenna patches what can severely deteriorate the convergence properties of the method. In this paper the studies are focused on microstrip/stripline structures, which can be characterized with the surface impedance boundary condition on the metallizations,

$$\vec{E}_s(x,y)|_{tan} = Z_F(x,y)\ \vec{J}_e(x,y) + \vec{E}_i(x,y)|_{tan}. \quad (1)$$

However, the method can also be extended on mixed structures consisting of both microstrip/stripline and coplanar/slotline components as presented in [15]. Based on equation (1), an integral equation for the surface currents can be formulated in the spectral domain,

$$\frac{1}{4\pi^2}\int_{k_y}\int_{k_x} \overleftrightarrow{G}^E_J\ (k_x,k_y)\cdot\vec{J}_e(k_x,k_y)e^{jk_xx+jk_yy}dk_xdk_y|_{tan}$$
$$= Z_F(x,y)\ \vec{J}_e(x,y) + \vec{E}_i(x,y)|_{tan} \quad (2)$$

where $\overleftrightarrow{G}^E_J\ (k_x,k_y)$ and $\vec{J}_e(k_x,k_y)$ are the Fourier transforms of the multilayered medium Green's function and the surface currents, respectively, whereas Z_F is a surface impedance and $\vec{E}_i$ comprises the excitation. The surface currents are discretized with subdomain basis functions $\vec{f}_m$ by,

$$\vec{J}_e(x,y) = \sum_{m=1}^{N} I_m\vec{f}_m(x,y). \quad (3)$$

At the moment asymmetric rooftop functions arranged on arbitrary nonuniform orthogonal meshes are used, which typically show also a sufficient modeling flexibility for geometries with oblique or curved margins, if suitable edge-meshing techniques are employed [16]. For the solution of the integral equation with the Galerkin testing procedure, equation (2) is multiplied by the basis functions itself. The subsequent integration over these testing functions $\vec{f}_n$ leads to,

$$\int_x\int_y \vec{f}_n(x,y)\cdot\vec{E}_s(x,y)dxdy =$$
$$\int_{k_y}\int_{k_x}\left[\ \overleftrightarrow{T}_{ll'}\ (k_x,k_y)\cdot\vec{F}_m(k_x,k_y)\right]\cdot\vec{F}^*_n(k_x,k_y)dk_xdk_y$$
$$, n\in g_l,\ m\in g_{l'}, \quad (4)$$

introducing a spectral domain translation operator between the groups g_l and $g_{l'}$

$$\overleftrightarrow{T}_{ll'}\ (k_x,k_y) = \overleftrightarrow{G}^E_J\ (k_x,k_y)e^{jk_x(x_l-x_{l'})}e^{jk_y(y_l-y_{l'})}. \quad (5)$$

Furthermore,

$$\vec{F}_{l'm}(k_x,k_y) = \int_x\int_y \vec{f}_m(x,y)e^{jk_x(x_{l'}-x)}e^{jk_y(y_{l'}-y)}dxdy \quad (6)$$

is the Fourier transform of the expansion function $\vec{f}_m$ related to the center $\vec{\rho}_{l'} = (x_{l'},y_{l'})$ of group $g_{l'}$ near this expansion function. Analogously $\vec{F}_{ln}(k_x,k_y)$ is the Fourier transform of the test function $\vec{f}_n$ related to the center $\vec{\rho}_l = (x_l,y_l)$ of group g_l near this test function.

To get a fast algorithm for the matrix-vector product evaluation,

$$Z_{far}\cdot\vec{I} = \vec{b}, \quad (7)$$

where Z_{far} is the matrix with the far interactions (not explicitly generated) and a similar efficiency as with standard fast multipole methods (FMM) in free space, the contribution to the elements of the right hand side of equation (7) $\vec{b} = (b_1,\ldots,b_n,\ldots,b_N)^T$ with regard to the groups g_l and g'_l is carried out by the integral,

$$b_{n,ll'} = \int_{k_x}\int_{k_y}\vec{F}^*_{ln}(k_x,k_y)\cdot\ \overleftrightarrow{T}_{ll'}\ (k_x,k_y)\cdot\vec{J}_{l'}(k_x,k_y)dk_x\,dk_y \quad (8)$$

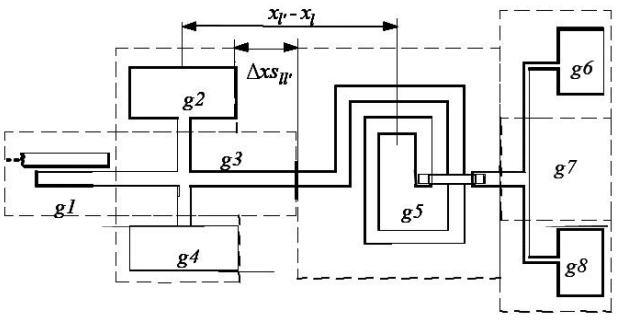

Fig. 1. Section of a typical microstrip structure with group decomposition and numbering.

which is evaluated numerically by,

$$b_{n,ll'} \approx \sum_{k_{xi},k_{yi}} w_{kxi}\, w_{kyi} \vec{F}^{*}_{ln}(k_{xi},k_{yi}) \cdot \overleftrightarrow{T}_{ll'}\,(k_{xi},k_{yi}) \cdot \vec{J}_{l'}(k_{xi},k_{yi}), \tag{9}$$

where k_{xi}, k_{yi} are suited sampling points of the cartesian wavenumber plane and w_{kxi}, w_{kyi} are appropriate integration weights.

In this representation, the spectral current density of all groups $g_{l'}$ with centers $\vec{\rho}_{l'}$ (source groups) is formed in the spectral domain by,

$$\vec{J}_{l'}(k_{xi},k_{yi}) = \sum_{m \in g_{l'}} I_m \vec{F}_{l'm}(k_{xi},k_{yi}), \quad l' = 1,\ldots,N_g \tag{10}$$

with N_g the number of groups. Equation (10) forms the aggregation process whereas equations (8) and (9) corresponds to the translation and disaggregation step, finally the elements of the complete right hand side of equation (7) are generated by,

$$b_n = \sum_{\substack{l' \neq l+NN \\ l'=1}}^{N_g} b_{n,ll'}, \quad l = 1,\ldots,N_g \tag{11}$$

where NN indicates near-neighbour groups.

However, if the spectral domain integrations equation (8) are carried out using standard quadrature techniques with real wavenumbers k_x and k_y, significant convergence problems occur due to integrand singularities, a slow decay and an oscillatory behavior of the integrands. To overcome these drawbacks, at first a special decomposition of the cartesian wavenumber plane is employed.

B. Decomposition of The Cartesian Wavenumber Plane

The decomposition of the cartesian wavenumber plane is shown in Fig. 2 together with the schematical arrangement of the sampling points k_{xi}, k_{yi}. The first quadrant is decomposed into an inner area A_{in} and three outer areas A_{out1} to A_{out3}. The other quadrants are decomposed analogously.

The Green's function contains singularities in terms of branchpoints and poles related to guided waves like surface or parallel plate waves. The localizations of guided wave poles and branchpoints are restricted by $|k_{xp}|, |k_{yp}| < k_0\sqrt{\epsilon_{r,max}}$, where k_{xp} and k_{yp} are the real locations of the singularities forming concentric rings within the inner areas and $\epsilon_{r,max}$ is the maximum permittivity of all layers. Furthermore, k_{Bx} and k_{By} denote the real locations of the branchpoints.

For the wavenumber k_x, the chosen integration path deformations in the inner areas are skeched in Fig. 3 a). The integration path extends from $-k_i$ on the real axis with a vertical and horizontal path section to $-jk_{xym}$, then through the origin along the branch cuts to $+jk_{xym}$ and finally to $+k_i$ back to the real axis. The choice for k_i is done with a numerical localization algorithm searching for the location $|k_{xpm}|$ of the pole with the largest propagation constant of the corresponding guided wave. Then the value k_i is chosen by $k_i \approx 1.1 \cdot |k_{xpm}|$ leading to a minimization of the inner area extension.

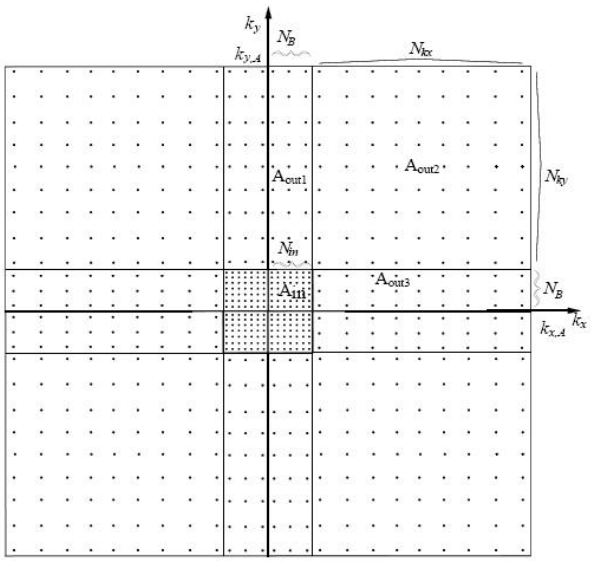

Fig. 2. Decomposition of the cartesian wavenumber plane with schematical distribution of sampling points.

This path is simultaneously used for the k_y-wavenumber.

C. Cancellation of Oscillatory Integrand Behavior

The integration paths in the inner area parallel to the real axis have the parametrization,

$$k_u(t_u) = t_u \pm jk_{xym}, \quad t_u \in [-k_i, k_i], \text{real}, \; u = x \text{ or } y. \tag{12}$$

The behavior of the integrands of equation (8) with regard to the variables t_x and t_y and the above integration paths can be well approximated by,

$$\mathrm{INT}_{n,ll'}(t_x,t_y) \approx C_{in} \vec{F}^{*}_{n}(t_x,t_y) \cdot \overleftrightarrow{G}^{E}_{J}\,(t_x,t_y) \cdot \vec{J}_{0l'}(t_x,t_y)\, e^{jt_x\,(x_l - x_{l'})}\, e^{jt_y\,(y_l - y_{l'})} \tag{13}$$

where $\vec{F}_n$ and $\vec{J}_{0l'}$ are now the Fourier transforms of the basis function $\vec{f}_n$ and the current distribution $\vec{J}_{l'}$ of group $g_{l'}$ with regard to the origin of the coordinate system (not to the group centers) and a factor C_{in} not depending on t_x and t_y. The terms $\vec{F}_n$ and $\vec{J}_{0l'}$ are actually evaluated in the implementation i.e., the translation operator $T_{ll'}$ is only implicitly involved to emphasize the analogies with fast multipole methods and to represent the integrand behavior.

Thus, the integrand mainly shows an oscillatory behavior due to the both exponentials containing the group center distances $(x_l - x_{l'})$ and $(y_l - y_{l'})$. To largely cancel out these oscillations, the product $\overleftrightarrow{T}_{ll'}$

$(k_x, k_y) \cdot \vec{J}_{l'}(k_x, k_y)$ is multiplied by the compensating exponentials $e^{-jt_x(x_l - x_{l'})}$ and $e^{-jt_y(y_l - y_{l'})}$. To account for these compensative multiplications, specific integration weights w_{txi}^{Leg}, w_{tyi}^{Leg} for the disaggregation process are determined.

If we emphasize on the integration with regard to t_x over an interval $t_x \in [t_{xa}, t_{xb}]$ and $F(t_x)$ is denoted as the smooth part of e.g., the integrand equation (13), we can write,

$$\int_{t_{xa}}^{t_{xb}} F(t_x) e^{jt_x(x_l - x_{l'})} dt_x \approx C_{sc} \sum_{i=0}^{N_{Leg}-1} F(t_{xi}) w_{txi}^{Leg} \tag{14}$$

where the weights w_{txi}^{Leg} of this special quadrature are the solutions of the linear system of equations,

$$\sum_{i=0}^{N_{Leg}-1} p_n(t_i)\ w_{txi}^{Leg} = \int_{-1}^{1} p_n(t) e^{j\,d\cdot t} dt,\ n = 0, \ldots, N_{Leg}-1 \tag{15}$$

with $p_n(t)$ denoting the Legendre polynomials of order n and t_i are the roots of the Legendre polynomial of order N_{Leg} (i.e the number of used sampling points), and $d = (t_{xb} - t_{xa})(x_l - x_{l'})/2$. Furthermore, we have introduced a scaling factor $C_{sc} = \frac{1}{2}(t_{xb} - t_{xa}) e^{j\frac{1}{2}(t_{xb}+t_{xa})(x_l - x_{l'})}$. Further details of the derivation and solution of equations (14) and (15) leading to this combined Legendre-Filon quadrature are given in [11]. The integration with regard to k_y is performed analogously.

On the vertical path sections on or parallel to the imaginary axis no oscillations occur, but we have an exponential increasing and decreasing behavior which becomes distinctive for large group distances. Therefore, this behavior is compensated as well by using a slightly modified integration technique as explained above. With these measures the number of sampling points N_{in} in the inner areas can be restricted to about 10-15 for both wavenumbers k_x, k_y using maximum group sizes of a few wavelengths.

D. Integration Path Deformations in The Outer Wavenumber Plane

These integrand oscillations are also present in the outer integration areas, if real wavenumbers k_x, k_y are employed. In this case the integrands of equation (8) behave like,

$$\begin{aligned} &\mathrm{INT}_{n,ll'}(k_x, k_y) \approx \\ &C_{out} \vec{F}_n^*(k_x, k_y) \cdot \overleftrightarrow{G}_J^E(k_x, k_y) \cdot \vec{J}_{0l'}(k_x, k_y) \\ &e^{jk_x(x_l - x_{l'})} e^{jk_y(y_l - y_{l'})}. \end{aligned} \tag{16}$$

Additionally, the Green's functions show a linear growing behavior with $k_x, k_y \to \infty$, if source and observation points are in the same plane $z = const$. Thus, convergence of the integrals is only achieved by the decay of the Fourier transforms of the group current distributions and the test basis functions.

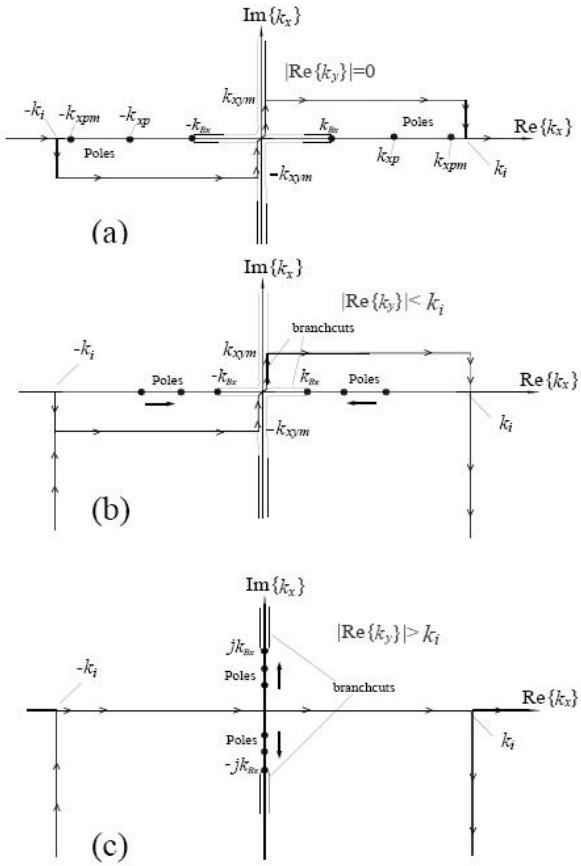

Fig. 3. Employed integration path deformations with singularity locations and migrations.

The overall convergence is therefore typically very poor and additionally depends on the group geometries. To achieve an extensive convergence acceleration, an adapted complex integration path deformation is employed in the outer areas. This integration path deformation depends on the values of the lateral group distances $|(x_l - x_{l'})|$ and $|(y_l - y_{l'})|$.

If $|(x_l - x_{l'})| > |(y_l - y_{l'})|$ is valid as given for the group arrangement in Fig. 4(a), the lateral group distance in x-direction causes the largest oscillations of the integrand equation (16). Choosing a complex integration path for the wavenumber k_x beginning from $k_x = \pm k_i$ according to,

$$k_x(t) = \pm k_i - jt,\ t \geq 0, \text{ real}, \tag{17}$$

then the corresponding oscillating exponential is transformed into a decaying exponential from this point,

$$e^{j\,k_x(t)(x_l - x_{l'})} = e^{\pm jk_i(x_l - x_{l'})} e^{-t\,(x_{l'} - x_l)} \tag{18}$$

provided that $(x_{l'} - x_l) > 0$.

However, it can be shown that an overall decay of the whole integrand equation (16) on the path equation (17) is only given if the group domains do not overlap with regard to this direction i.e., if we have a finite separation with a distance $\Delta xs_{ll'} > 0$ (see Fig. 1 and Fig. 4(a)). As will be shown later, the decay behavior of the integrand equation (16) for larger values t in equation (17) is dominated by the exponential $e^{-t\Delta xs_{ll'}}$. Therefore, the following case differentiation is made:

If $|\Delta xs_{ll'}| > |\Delta ys_{ll'}|$ (see Fig. 4(a)), then a complex integration path for k_x is used according to equation (17) whereas k_y remains real in the outer areas.

If $|\Delta ys_{ll'}| > |\Delta xs_{ll'}|$ (see Fig. 4(b)), then the complex integration path for k_y,

$$k_y(t) = \pm k_i - jt,\ t \geq 0, \text{ real}, \tag{19}$$

is used, whereas k_x remains real, correspondingly the integrand decay is dominated by $e^{-t|\Delta ys_{ll'}|}$ in this case.

If the first case is valid, $\Delta xs_{ll'}$ must not be negative i.e., the observation group must be located left from the source group. Analogously, $\Delta ys_{ll'}$ must not be negative in the second case i.e., the observation group must be located below the source group. If these geometrical configurations are not fulfilled, the roles of source and observation groups are simply exchanged. This means, that in these cases the aggregation step equation (10) extends over the conjugate complex Fourier transforms $\vec{F}^*_{ln}(k_{xi}, k_{yi})$ whereas the disaggregation step equation (9) is performed with the simple Fourier transforms $\vec{F}_{l'm}(k_{xi}, k_{yi})$.

An overview of the pole and branchpoint migration together with the introduced integration path deformations for the wavenumber k_x is given in Fig. 3(b) and (c). Figure 3(b) shows the circumstances for the case $0 < \mathrm{Re}(k_y) < k_i$. In this case, the poles due to guided waves and the branchpoints $\pm k_{Bx}$ are located near the real axis. Thus, they are circumvented by the rectangularly shaped integration path of the inner areas. Beginning from $k_x = \pm k_i$, the integration paths proceed parallel to the imaginary axis. If $\mathrm{Re}(k_y)$ becomes larger, the poles and branchpoints migrate towards the origin. In the case $\mathrm{Re}(k_y) > k_i$ (Fig. 3(c)) they proceed together with the branchcuts on the imaginary axis. Therefore the rectangularly shaped integration path can be replaced by a path on the real axis in this case. The significant advantage of this choice of path deformation is given by the fact, that no poles and branchcuts are crossed, thus no residue contributions must be considered.

However, despite of the exponential decay behavior achieved by the introduced complex integration paths, an oscillating exponential always remains e.g., in the case $|\Delta xs_{ll'}| > |\Delta ys_{ll'}|$, the term $e^{jk_y(y_l - y_{l'})}$ must be considered. Furthermore, we have a larger number of oscillation cycles in the outer areas compared to the inner areas, since the integration intervals are larger than in the inner areas (see Fig. 1). Applying the Legendre-Filon quadrature outlined above during the disaggregation process, the exponential $e^{-jk_y(y_n - y_{l'})}$ is used for the compensation of the oscillations with regard to k_y instead of $e^{-jk_y(y_l - y_{l'})}$. Here, $\vec{\rho}_n = (x_n, y_n)$ denotes the lateral location of the individual test basis function $\vec{f}_n(x, y)$ with regard to the origin of the main coordinate system. With this individual treatment of each test function during the disaggregation process, the best oscillation suppression is reached what is especially important for larger groups.

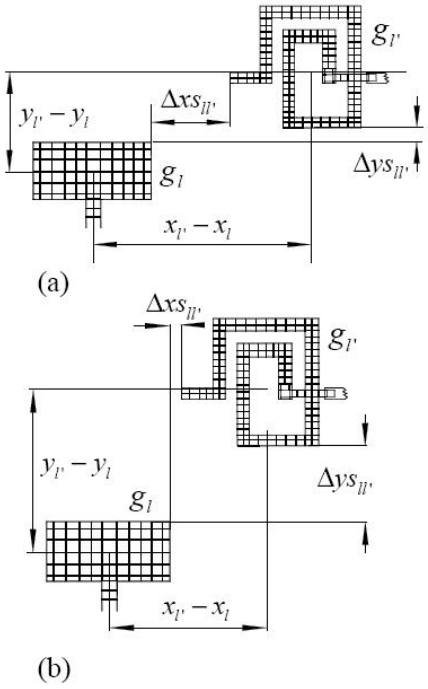

Fig. 4. Group constellations in context with integration path deformations in the outer areas.

The additional effort for computing the quadrature weights for the individual test functions is practically negligible. Although we have no exponential decay for the integrand with regard to the remaining real wavenumber, the upper integration boundary $k_{x,A}, k_{y,A}$ can be restricted to about $15\,k_0$ with a number of sampling points N_{kx}, N_{ky} of about 5-8.

E. Extended Laguerre Quadrature Applied to The Outer Integrands

Now the integrals over the outer areas already show excellent convergence properties due to the outlined integration path deformations and quadrature techniques. However, the exponential decay rate on the paths equations (17) and (19) strongly depends on the non-overlapping group distances $\Delta xs_{ll'}$ or $\Delta ys_{ll'}$, which is a severe drawback for an integration technique using a rigid sampling point distribution.

The essential decay behavior of the group interaction integrands is demonstrated in Fig. 5 (a), depicting a linear

patch array with 6 patches where each patch is considered as one group. If we consider the interactions of group 1 with the other groups, then the first non-neighbour group is the third one in this case, leading to the minimum non-overlapping group distance $\Delta xs_{min} = \Delta xs_{13}$, providing the slowest decay rate. To analyze the essential decay behavior of the group interaction integrands, the patch currents are described by one symmetric rooftop function for each patch. The exponential behavior of the Fourier transform with regard to k_x of such a rooftop function is simply given by,

$$F_{l'}(k_x) = \Big(w - \frac{w}{2}(e^{j\frac{w}{2}k_x} + e^{-j\frac{w}{2}k_x})\Big)e^{jx_{l'}k_x} \qquad (20)$$

i.e., the further dependence $\sim \frac{1}{k_x^2}$ is not considered here. The exponential behavior of the interaction integrand of observation group 1 with the other non-neighbour source groups is then defined by $\mathrm{INT}_{1l'}(k_x) = F_1^*(k_x)\, F_{l'}(k_x)$, $l' = 3, \ldots, 6$, i.e., the influence of the Green's function is neglected for this representation. Figure 5(b) shows the behavior of the interaction integrands $\mathrm{INT}_{1l'}(k_x)$ and of the exponential $e^{-k_x \Delta xs_{1l'}}$ on the path $k_x = k_i - j\,t$ with $w = 12$ mm, $\Delta x_{12} = 5$ mm, $f = 10$ GHz and $k_i = \sqrt{2.2}k_0$. All curves are normalized to 0 dB for $t = 0$. As expected it can be recognized that the decay rate of the integrands for small values of t is even larger than the decay rate of the corresponding exponential $e^{-k_x \Delta xs_{1l'}}$, but for larger t both expressions quickly show the same decay rate.

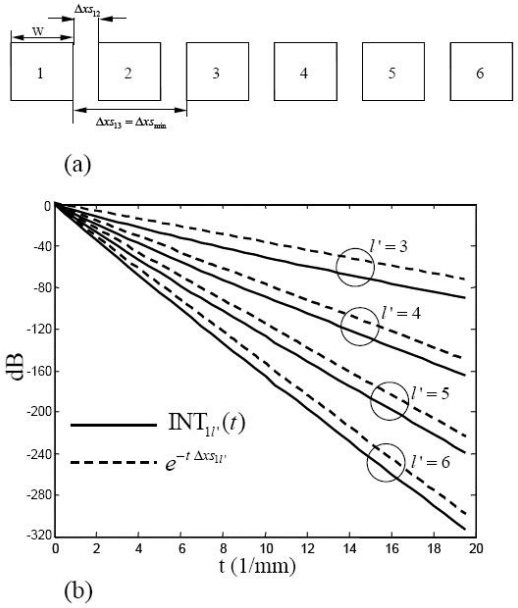

Fig. 5. Linear test array (a) and the decay behavior of the corresponding interaction integrands (b).

If the sampling points for the integration are adjusted to the slowest decay rate with regard to a chosen group decomposition, the integrands with significantly faster decay rates cannot be evaluated with sufficient accuracy applying these sampling points. To get rid of these different decay rates, the products $\overleftrightarrow{T}_{ll'}(k_x, k_y) \cdot \vec{J}_{l'}(k_x, k_y)$ are multiplied by corresponding increasing exponentials $e^{+t\,\alpha}$, where for small separations $\alpha = \Delta xs_{min}$ is chosen and $\alpha = \Delta xs_{ll'}$ for all separations larger than $\approx 2\Delta xs_{min}$.

To account for these multiplications, again special integration weights are determined. If we emphasize on the integration with regard to k_x on the path equation (17) and using the substitution $t' = \Delta xs_{min}\, t$ it can be written,

$$I = \int_0^\infty F(k_x(t))e^{-\Delta xs_{ll'}t}dt =$$
$$\frac{1}{\Delta xs_{min}} \int_0^\infty F\big(k_x(\frac{t'}{\Delta xs_{min}})\big)e^{-\left(\frac{\Delta xs_{add}}{\Delta xs_{min}}+1\right)t'}dt' \approx$$
$$\frac{1}{\Delta xs_{min}} \sum_{s=0}^{N_{Lag}-1} F\big(k_x(\frac{t_s}{\Delta xs_{min}})\big)w_s^{Lag} \quad . \qquad (21)$$

$F(k_x)$ denotes the smooth decaying part of the integrand and $\Delta xs_{ll'} = \Delta xs_{min} + \Delta xs_{add}$ was used. In the case of a group interaction with the minimum separation Δxs_{min} (i.e., $\Delta xs_{add} = 0$), the exponential of the second integral in equation (21) becomes $e^{-t'}$. Such weighting function is related with the standard Laguerre quadrature, thus the weights w_s^{Lag} can be directly derived with this quadrature rule in this case. The sampling points t_s are the roots of the Laguerre polynomial of order N_{Lag}. However, this quadrature becomes less accurate for separations $\Delta x_{ll'}$ larger than about $2\Delta xs_{min}$. For these cases, extended Laguerre quadrature weights are computed, using a similar variational approch as for the outlined Legendre-Filon quadrature. This leads to the linear system of equations,

$$\sum_{s=0}^{N_{Lag}-1} l_n(t_s)w_s^{Lag} = \int_0^\infty l_n(t)e^{-\left(\frac{\Delta xs_{add}}{\Delta xs_{min}}+1\right)t}dt,$$
$$n = 0, \ldots, N_{Lag} - 1 \qquad (22)$$

where $l_n(t)$ are the Laguerre polynomials of order n using the same sampling points t_s as the standard Laguerre quadrature. The right hand side is efficiently computed by means of the integral $\int_0^\infty t^n\, e^{-\alpha\, t}dt = n!/\alpha^{n+1}$. By this quadrature technique, all contributions with exponential decay can be evaluated with the same sampling points and accuracy. The number of necessary sampling points N_{kx} and N_{ky} on the paths equations (17) and (19) amounts to approx. 5–7 and can be further reduced for interactions with large separations.

F. Near-Zone Matrix and Preconditioning Stategies

While the interactions between the well separated groups can be computed by the methods described above, the interactions between near-neighbour groups must be evaluated directly by computing the matrix entries of the standard MoM. This is done with the methods outlined in [11] based on an asymptotic extraction technique for convergence acceleration. However, it can be noted that the outlined integration techniques given above can also be applied for the computation of the standard MoM matrix entries with high accuracy and efficiency, if the participated basis functions do not overlap.

The entries of this near-zone matrix Z_{near} are stored in the compressed sparse row (CSR) format (see e.g., [17]). This near-zone matrix is also used to build a preconditioner for the pertinent Krylov subspace solvers. At first, a Transpose Free Quasi Minimim Residual (TFQMR) method was employed [18], showing already very good convergence properties, but the currently implemented Generalized Minimum Residual (GMRES)-solver shows so far the best convergence for a large class of structures.

If we have a pure microstrip or aperture structure, the system matrix is symmetric, thus a sparse Cholesky factorization of the near-zone matrix is applied,

$$Z_{near} = C \cdot C^T. \tag{23}$$

For this factorization a special kind of sparse LDL^T-factorization based on a pure row-wise access on the matrix entries is used at first. This LDL^T-factorization is subsequently transformed into the desired Cholesky factorization, which is stored in the modified sparse row (MSR) format. Furthermore, matrix fill-ins are permitted during the factorization process, whereas the number of these matrix fill-ins is reduced by a proper group numbering in advance. The localizations of the fill-ins are determined during a symbolic factorization to guarantee a correct storage allocation.

This Cholesky factorization is subsequently used as a split preconditioner according to,

$$C^{-1}\, Z\, C^{-T}\; C^T \cdot \vec{I} = C^{-1} \cdot U, \quad Z = Z_{far} + Z_{near}. \tag{24}$$

The required forward/backward substitutions to carry out equation (24) are as well implemented using a pure row-wise access on the entries of the Cholesky factorization. Since the groups can also be interpreted as so-called macro basis functions of the structure within diakoptic strategies [13,19], we refer to the explained techniques also as a diakoptic preconditioning.

III. APPLICATIONS

For a first validation, the bistatic radar cross section (RCS) of a 4x4 patch array on a grounded dielectric slab is analyzed (Fig. 6(a)).

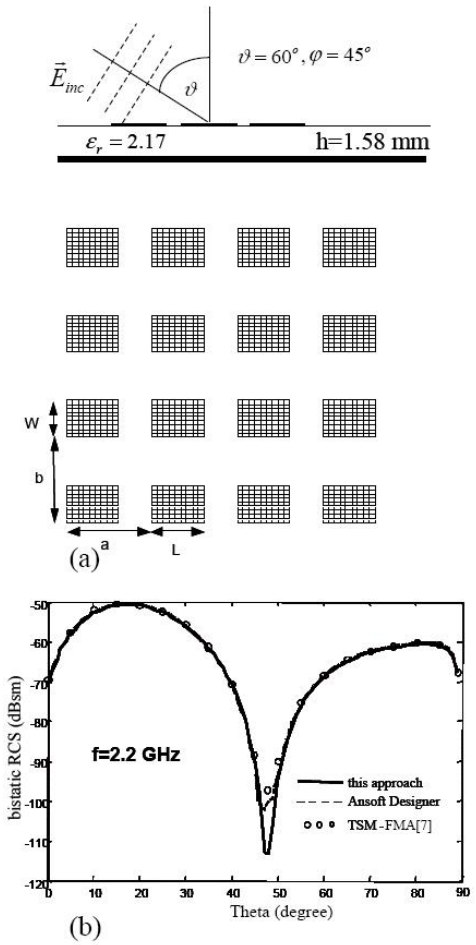

Fig. 6. Reflectarray (a) and bistatic RCS computations with different methods (b); a=b=60.0 mm, W=26.0 mm, L=36.6 mm.

Similar as in [8], where the structure was examined at first, a homogeneous discretization was chosen with 2300 unknowns altogether. Each patch was considered as one group. Additionally, the structure was analyzed with the Planar-EM solver of Ansoft Designer with about the same number of RWG (Rao Wilton Glisson) basis functions.

The comparison of the bistatic RCS ($\vartheta - \vartheta$) in Fig. 6(b) shows a very good agreement, only the behavior around the minimum of the RCS at about 48 degrees is predicted slightly different by the three methods. However, the overall computation time of this approach amounts to only 2.5 sec. (3 GHz AMD-PC, used for all examples), whereas more than 30 sec. are needed with the solver of Ansoft Designer on the same computer.

As a second example a microstrip antenna array with feeding network consisting of up to four subarrays with 32 elements is considered. Figure 7 (a) shows the structure geometry and the discretization using an edge-meshing for the patches. Further details of the geometry parameters are given in [11,5]. Each subarray was decomposed into 9 groups as indicated by the dashed rectangles by hands

of the first subarray. Figure 7 (b) shows the current distribution at 9.42 GHz.

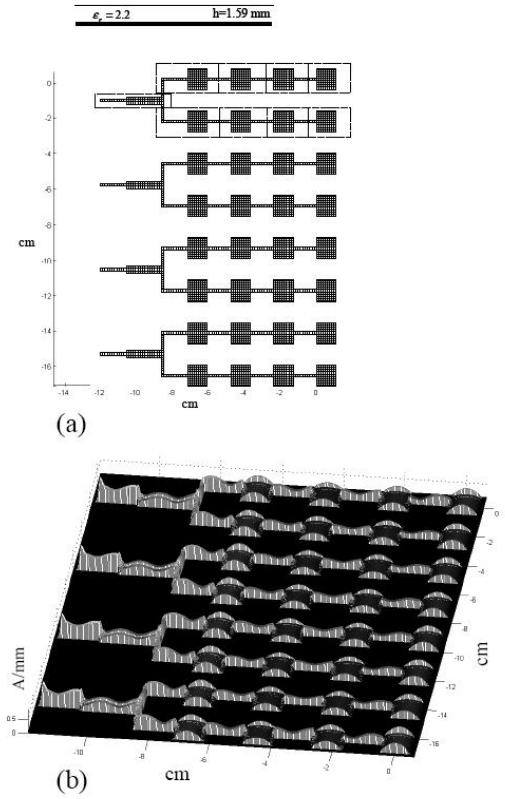

Fig. 7. Microstrip antenna array (a) with computed current distribution (b).

For results and performance comparisons, the structure was analyzed with Ansoft Designer as well using about the same number of unknowns. Using our diakoptic preconditioner and GMRES implementation, only 2-3 iterations are needed for a residual error of less than 1 percent. Table 1 shows the comparison of the overall solution time in seconds depending on the number of subarrays and unknowns N.

Table 1. Comparison of the numerical performance for a microstrip antenna array.

subarrays (N)	This approach	Ansoft Designer
1 (1625)	5	19
2 (3250)	12	55
3 (4875)	24	115
4 (6500)	38	131(fast solver)

It can be recognized that this approach is up to more than four times faster than the simulations of Ansoft Designer. In the case of four subarrays, Ansoft Designer makes use of a fast matrix compression algorithm using multilevel strategies, based on a singular value decomposition (SVD) [20] indicated with fast solver in the table. However, the application of this method is only advantageous for problems with more than 5000 unknowns, whereas the approach proposed in this paper shows an increased efficiency already for small problems.

Figure 8 shows the results for the far-field antenna patterns. Whereas the E-plane patterns show slight differences between both methods, the H-plane patterns are nearly congruent except for minor deviations at $\pm$ 40 degrees. However, the pattern results are also influenced by the meshing modalities to some extend.

As a final example, the monostatic RCS of larger reflectarrays is examined, first characterized in [21] with an entire domain approach. Figure 9 shows the largest array with 11x11 patches together with the used discretization of 17182 unknowns and a typical group decomposition indicated by the dashed rectangles. For an accurate current description, again an edge-meshing was applied.

A comparison of the numerical performance of this approach and Ansoft Designer in terms of overall solution time in seconds is given in Table 2.

Table 2. Comparison of the numerical performance for two reflectarrays.

array type (N)	This approach	Ansoft Designer
7x7 (6958)	12-25	138 (fast solver)
11x11 (17182)	60-139	650 (fast solver)

However, for the fast spectral domain solver the necessary number of iterations and therefore the solution time depends on frequency, whereas nearly the same time is needed by Ansoft Designer for all frequency points. For the fast spectral domain approach, the worst convergence appears at the resonance frequencies with 4-6 necessary iterations, whereas for the remaining frequencies only 2-3 iterations are required for a residual error of less than 1 percent. Although the fast spectral domain approach is currently based only on a two-level strategy, it is up to one magnitude faster than the multilevel algorithms of Ansoft Designer.

The results for the monostatic RCS ($\vartheta - \vartheta$) are given in Fig. 10(a) for the three methods. The curves of this approach and Ansoft Designer are nearly congruent, whereas slight differences are observed for the entire domain method especially at the first patch resonance around 2.71 GHz and the minimum at about 3.25 GHz. Due to the incident angle of $\varphi = 45^o$ of the exciting plane wave, both patch resonances are excited as illustrated by hands of the current distribution (this approach) in Fig. 10(b) (first resonance) and Fig. 10(c) (second resonance).

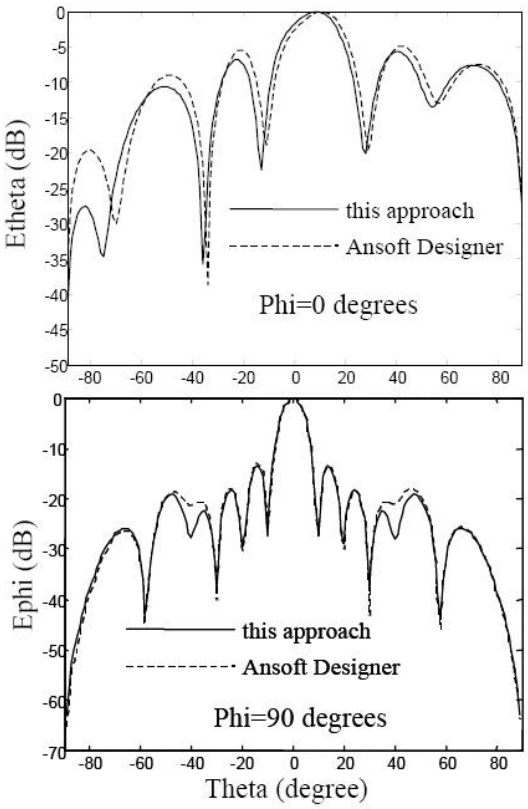

Fig. 8. Far-field pattern comparison for the antenna array of Fig. 7.

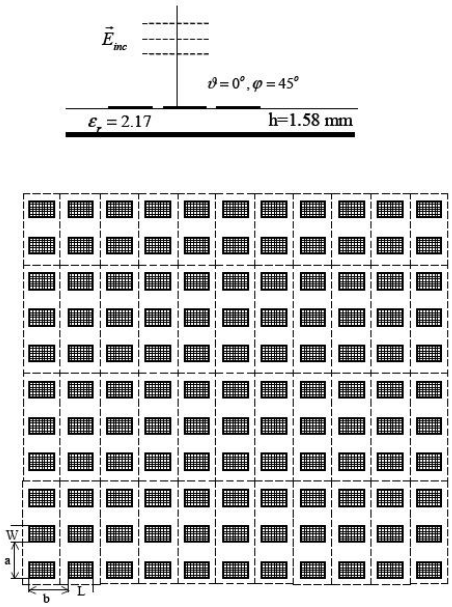

Fig. 9. Reflectarray with 11x11 patches with discretization and group decomposition; a=b=55.517 mm, W=26.0 mm, L=36.6 mm.

The detailed numerical behavior of the fast spectral domain solver is given in Fig. 11 based on computations of reflectarrays of 3x3 elements up to 11x11 elements with three iterations. Additionally the behavior of Ansoft Designer is outlined. As indicated in the diagramms, Ansoft Designer uses a standard MoM up to 5000 unknowns (6x6-array) and switches over to its fast matrix compression algorithm (fast SVD solver) beginning with the 7x7-reflectarray. According to [20], the numerical complexity of this fast SVD solver should reach $O(N \log N)$ concerning the matrix-vector product evaluation (Fig. 11(a)).

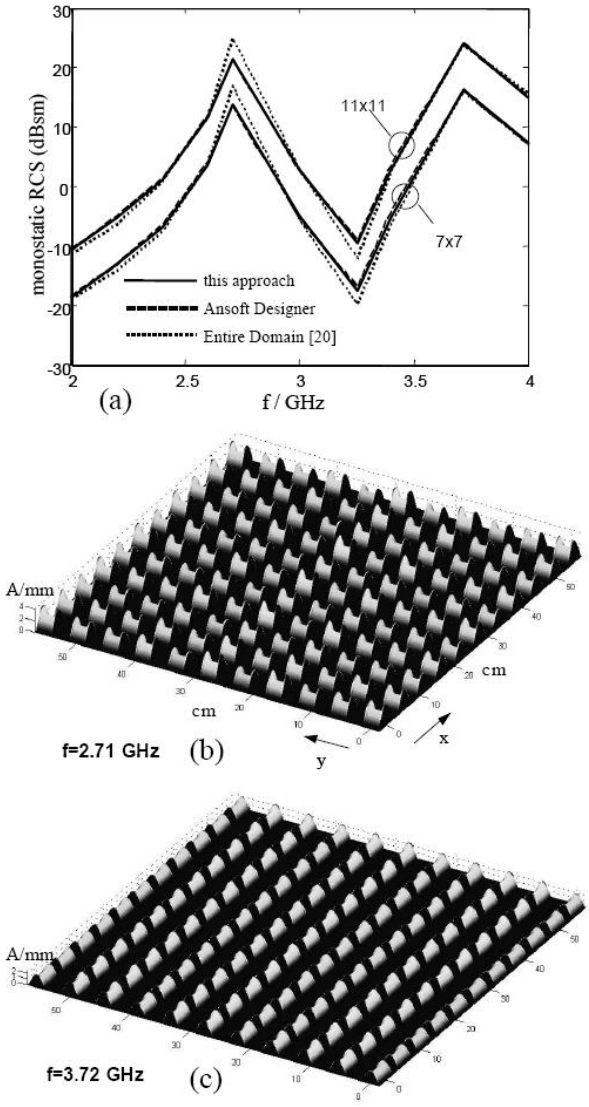

Fig. 10. Comparison of the monostatic RCS of the 11x11 reflectarray (Fig. 9) and a 7x7 reflectarray computed with different methods (a). Computed current distribution at the fist (b) and second patch resonance (c).

Since the necessary number of iterations increases noticeably with increasing number of unknowns, the overall numerical complexity of Ansoft Designer (solid line) is obviously larger than $O(N \log N)$. In contrast to this, the number of necessary iterations remains roughly constant

using the fast spectral domain solver, thus the complexity is only slightly higher than $O(N^{1.5})$. This slightly higher complexity is caused by the additional computation of the sparse Cholesky factorization and the forward-backward substitutions in conjunction with the employment of the diakoptic preconditioning. Figure 11(b) shows the memory requirements of both approaches. Whereas the storage complexity of this approach is slightly higher than $O(N)$, the memory requirement of Ansoft Designer shows a quite complicated behavior, but is typically significantly higher than observed with this approach.

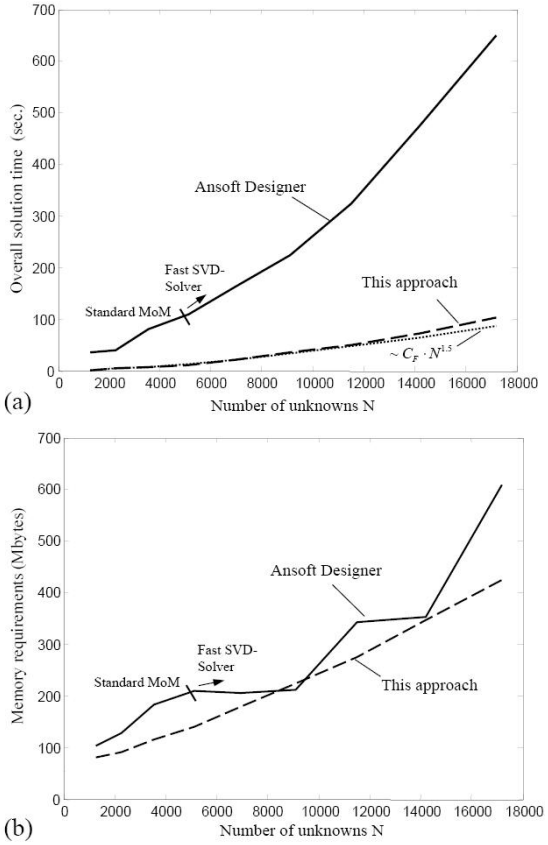

Fig. 11. Comparison of the overall computation time versus number of unknowns (a); Behavior of the storage requirements (b).

The same structures were also analyzed in [7] with a fast multipole approach based on a modified complex discrete image method using a Pentium IV 2.4 GHz PC. In [7], a 3x3 and a 7x7 array with 1737 and 8428 unknowns was computed with 0.6 seconds and 7.49 seconds per iteration, respectively. If we consider the lower clock rate of the computer used in [7], this would result in roughly the same computational effort with 0.54 seconds and 7.47 seconds per iteration using this approach and the same number of unknowns.

IV. CONCLUSIONS

This paper has introduced a new kind of fast spectral domain solver for the characterization of larger microwave structures embedded in arbitrary multilayered media with a similar numerical complexity than fast multipole methods for structures in free space. The group interactions within the fast matrix-vector product computations are evaluated in the cartesian wavenumber plane, where adaptive integration path deformations and enhanced integration techniques such as higher-order Legendre-Filon and extended Laguerre quadrature rules lead to a high accuracy with a low integration effort. Together with diakoptic preconditioning techniques, a fast convergence of the pertinent Krylov subspace solvers is achieved, leading to a very good overall numerical performance of the whole framework. This is demonstrated by means of several applications and comparisons with other solvers, showing a significantly higher computational performance than a comparable commercial software package whereas a similar performance is observed in comparison with a fast multipole method modified for the treatment of multilayered media. The next investigations aim for a substantial reduction of quadrature points by an optimization of the integration path deformations and a further improved treatment of the evanescent wave contributions.

REFERENCES

[1] T. K. Sarkar, E. Arvas, and S. S. Rao, "Application of FFT and conjugate gradient method for the solution of electromagnetic radiation from electrically large and small conducting bodies," *IEEE Trans. Microwave Theory Tech.*, vol. 34, pp. 635–640, May 1986.

[2] M. F. Catedra, J. G. Cuevas, and L. Nuno, "A Scheme to Analyze Conducting Plates of Resonant Size Using the Conjugate-Gradient Method and the Fast Fourier Transform," *IEEE Trans. Antennas Propagat.*, vol. 36, no. 12, pp. 1744–1752, Dec. 1988.

[3] J. Basterrechea and M. F. Catedra, "Electromagnetic Analysis of Complex Microstrip Structures Using a CG-FFT scheme," *IEEE MTT-S Symp. Dig.*, vol. 35, no. 8, pp. 991–996, Aug. 1987.

[4] Y. Zhuang, K.-L. Wu, C. Wu, and J. Litva, "A combined full-wave CG-FFT method for rigorous analysis of large microstrip antenna arrays," *IEEE Trans. Antennas Propagat.*, vol. 44, no. 1, pp. 102–109, Jan. 1996.

[5] F. Ling, C.-F. Wang, and J.-M. Jin, "An efficient algorithm for analyzing large-scale microstrip structures using adaptive integral method combined with discrete complex-image method," *IEEE Trans. Microwave Theory Tech.*, vol. 48, pp. 832–838, May 2000.

[6] P. A. Macdonald and T. Itoh,"Fast simulation of microstrip structures using the fast multipole method," *Int. J. Numer. Modell. Electron. Networks Devices Fields*, no. 9, pp. 345–357, 1996.

[7] J. X. Wan, T. M. Xiang, and C. H.Liang, "The fast multipole algorithm for analysis of large-scale microstrip antenna arrays," Progress in Electromagnetic Research, Pier 49, pp. 239–255, 2004.

[8] J.-S. Zhao, W. C. Chew, C.-C. Lu, E. Michielssen, and J. Song, "Thin-stratified medium fast-multipole algorithm for solving microstrip structures," *IEEE Trans. Microwave Theory Tech.*, vol. 46, no. 4, pp. 395–403, April 1998.

[9] B. Hu and W. C. Chew, "Fast inhomogeneous plane wave algorithm for electromagnetic solutions in layered medium structures: Two dimensional case," *Radio Science*, vol. 35, no. 1, pp 31–43, Jan.-Feb. 2000.

[10] D. V. Ginste, E. Michielssen, F. Olyslager, and D. De Zutter, "An efficient perfectly matched layer based multilevel fast multipole algorithm for large planar microwave structures," *IEEE Trans. Antennas Propagat.*, vol. 54, no. 5, pp. 1538–1548, May 2006.

[11] T. Vaupel, T. F. Eibert, and V. Hansen, "Spectral domain analysis of large (M)MIC-structures using novel quadrature methods," *Int. Journal of Num. Modelling: Electronic Networks, Devices and Fields*, Jan.-Febr., pp. 23–38, 2005.

[12] M. S. Garino, G. Vecchi, and M. Orefice, "Efficient spectral evaluation of mutual coupling between planar antennas," *Radio Science*, vol. 35, no. 2, pp. 511–523, March-April 2000.

[13] T. Vaupel, T. F. Eibert, and V. Hansen, "Diakoptic basis function grouping techniques applied to the method of moment solution of (M)MIC-structures," *IEEE AP Symposium Digest 2003*, Columbus, Ohio, vol. 2, pp. 1059–1062.

[14] W. C. Chew, J.-M. Jin, E. Michielsen, and J. Song, *Fast and Efficient Algorithms in Computational Electromagnetics*, Boston, MA: Artech House, 2001.

[15] T. Vaupel and V. Hansen, "Electrodynamic analysis of combined microstrip and coplanar/slotline structures with 3-D components based on a surface/volume integral-equation approach," *IEEE Trans. Microwave Theory Tech.*, vol. 47, no. 9, pp. 1788–1800, Sep. 1999.

[16] T. Vaupel and T. F. Eibert, "Recent developments and applications of a spectral domain planar-3D solver," *4th European Workshop on Conformal Antennas*, Stockholm, Sweden, pp. 71–74, May 23-24 2005.

[17] Y. Saad, *Iterative methods for sparse linear systems*. SIAM books, 2nd edition, 2000.

[18] R. W. Freund, "Conjugate gradient-type methods for linear systems with complex symmetric coefficient matrices," *SIAM J. Sci. Stat. Comput.*, vol. 13, no. 2, pp. 425–448, especially p. 429, Jan. 1992.

[19] S. Ooms and D. De Zutter, "A new iterative diakoptics-based multilevel moments method for planar circuits," *IEEE Trans. Microwave Theory Tech.*, vol. 46, no. 3, pp. 280–291, March 1998.

[20] S. Kapur and D. Long, "IES^3: A fast integral equation solver for efficient 3-Dimensional extraction," *IEEE/ACM International Conference on Computer-Aided Design*, pp. 448-455, Nov. 1997.

[21] A. S. King and W. J. Bow, "Scattering from a finite array of microstrip patches," *IEEE Trans. Antennas Propagat.*, vol. 40, no. 7, pp. 770–774, July 1992.